Fuel Cells

DOI: 10.1002/anie.201406812

Confined-Space Alloying of Nanoparticles for the Synthesis of Efficient PtNi Fuel-Cell Catalysts**

Claudio Baldizzone, Stefano Mezzavilla, Hudson W. P. Carvalho, Josef Christian Meier, Anna K. Schuppert, Marc Heggen, Carolina Galeano, Jan-Dierk Grunwaldt, Ferdi Schüth, and Karl J. J. Mayrhofer**

Abstract: *The efficiency of polymer electrolyte membrane fuel cells is strongly depending on the electrocatalyst performance, that is, its activity and stability. We have designed a catalyst material that combines both, the high activity for the decisive cathodic oxygen reduction reaction associated with nanoscale Pt alloys, and the excellent durability of an advanced nanostructured support. Owing to the high specific activity and large active surface area, the catalyst shows extraordinary mass activity values of 1.0 A mg_{Pt}^{-1}. Moreover, the material retains its initial active surface area and intrinsic activity during an extended accelerated aging test within the typical operation range. This excellent performance is achieved by confined-space alloying of the nanoparticles in a controlled manner in the pores of the support.*

In a world searching intensively for sustainable energy solutions, proton exchange membrane (PEM) fuel cells are promising candidates for efficient energy conversion of stored chemical energy into electrical energy. However, if they are to be considered as a viable alternative technology, such devices have to overcome some important shortcomings. Among these issues is the sluggish rate of the oxygen reduction reaction (ORR), which is the main reason for the high loading of noble-metal catalyst and thus the still too high costs of the device.[1] Therefore, numerous catalysts have been developed to increase the electrochemically active surface area (ECSA) by utilizing finely dispersed nanoparticles[2] and/or to enhance the intrinsic ORR activity by alloying Pt with 3d-transition metals as the most promising approach.[3] This high catalyst activity is crucial for the efficiency of electrochemical reactors, but at least equally important for applications is its conservation over an extended operational time of often more than 5000 h.[1a,4] Consequently, great efforts have recently been directed towards the investigation of catalyst degradation, leading to a more comprehensive understanding of catalyst performance.[4,5] Promising developments for Pt alloy fuel cell catalysts are based on, for instance, nanostructured thin films (NSTF), which are currently among the best performing materials and thus serve as a benchmark for further developments according to the US Department of Energy.[1a,6]

To go beyond this benchmark, several approaches have been followed, relying on alloys with different particle size, shape and composition,[7] as well as on different support materials.[8] An extended comparison of activity and stability of some of the most advanced Pt alloy catalysts reported is provided in the Supporting Information.[6,9]

Generally a particle size around 3–5 nm with a narrow size distribution and compositional homogeneity is considered to be most beneficial for the catalyst performance. However, the synthesis of alloy particles by conventional methods—co-precipitation of the components and subsequent high-temperature annealing, or solvothermal synthesis of alloy nanoparticles followed by deposition on the support—can lead to uncontrolled agglomeration and particle growth, or to insufficient attachment of the nanoparticles to the support, respectively.

Herein we report the synthesis of a highly active and stable class of catalysts by confined-space alloying. The system chosen is PtNi nanoparticles embedded in a special 3D mesoporous structure, in the shape of graphitic hollow spheres (HGS). The same graphitic structure has already been used to incorporate Pt nanoparticles, and it was found to be pivotal in assuring an optimal spatial distribution of the nanoparticles during the synthesis and in suppressing some of the electrochemical degradation pathways, such as agglomeration and detachment, during the ORR in both fundamental

[*] C. Baldizzone,[+] Dr. J. C. Meier, Dr. A. K. Schuppert, Dr. K. J. J. Mayrhofer
Department of Interface Chemistry and Surface Engineering
Max-Planck-Institut für Eisenforschung GmbH
Max-Planck-Strasse 1, 40237 Düsseldorf (Germany)
E-mail: mayrhofer@mpie.de

S. Mezzavilla,[+] Dr. C. Galeano, Prof. Dr. F. Schüth
Department of Heterogeneous Catalysi
Max-Planck-Institut für Kohlenforschung
Kaiser-Wilhelm-Platz 1, 45470 Mülheim an der Ruhr (Germany)

Dr. H. W. P. Carvalho, Prof. Dr. J.-D. Grunwaldt
Institute for Chemical Technology and Polymer Chemistry and
Institute of Catalysis Research and Technology
Karlsruher Institut für Technologie (KIT)
Kaiserstrasse 12 76131 Karlsruhe (Germany)

Dr. M. Heggen
Ernst Ruska Center for Microscopy and Spectroscopy with Electrons, Forschungzentrum Jülich GmbH
52425 Jülich (Germany)

[+] These authors contributed equally to this work.

[**] We thank the DFG for the financial support through DFG/AiF-Cluster "Innovative Materialen und Verfahren für MT-PEM-Brennstoffzellen". Dr. C. Weidenthaler is gratefully acknowledged for the support in the XRD measurements. We also thank Dipl.-Ing. A. Mingers for the help in the ICP-MS measurements. C.B. acknowledges financial support from the IMPRS-SurMat doctoral program. We acknowledge the ANKA radiation synchrotron facility for proving beamtime at the XAS beamline.

Supporting information for this article is available on the WWW under http://dx.doi.org/10.1002/anie.201406812.

rotating disc electrode (RDE) as well as single fuel-cell studies.[10] In this work we demonstrate that the pore-confinement effect, ensured by the mesoporous structure of the HGS support material, can be effectively exploited to alloy Pt–Ni catalysts at high temperatures, exceeding 800 °C, without losing valuable active surface area. Owing to the resulting extraordinary high mass activity for the ORR, combined with the high stability provided by this type of support, this class of catalysts opens up an attractive new direction for improving long-term fuel-cell performance.

The HGS synthesis followed the procedure presented in our previous work.[10a] The metal precursors are simultaneously introduced in the pores of the carbon support through an ultrasound-assisted incipient wetness impregnation, and they are reduced to the metallic state under a H_2/Ar gas mixture. At this stage, the metal nanoparticles resemble the features of metal clusters (1.6 ± 0.3 nm) homogeneously distributed all over the carbon support (see Figure S2 in the Supporting Information), as confirmed by the broad reflection present in the X-ray diffraction (XRD) pattern (Figure 1 A). The annealing treatment promotes some sintering of the clusters, owing to migration and coalescence of clusters located in proximity to each other within the pore system of the HGS. Despite the harsh conditions used in the annealing treatment, that is, high temperature (850 °C) and long dwell time (7 h), the particles retain an exceptionally small size (3.5 ± 0.7 nm). The mesoporous structure physically confines the metal particles which is associated with multiple advantages: 1) it allows the formation of an alloy catalyst at high temperatures; 2) it determines the final size of the nanoparticles preventing their extensive sintering which occurs with other mesoporous supports in catalysis,[11] and 3) it ensures an excellent spatial distribution of the PtNi nanoparticles.

The XRD pattern measured after the alloying treatment (Figure 1 A) shows a moderate sharpening of the reflections, in agreement with the controlled growth of the nanoparticles visible in TEM analysis (Figure 1 C, D and Figure S2B). The reflections can be assigned to a disordered fcc PtNi (1:1) structure with shifted—compared to pure platinum—(111), (200), (220), (311), and (222) reflections, resulting from the insertion of Ni atoms into the Pt lattice. The structural model derived from the analysis of the extended X-ray absorption fine structure (EXAFS) spectra at the Pt L_3-edge and Ni K-edge (Figure 2 A–C) confirms the presence of 2–3 nm disordered alloy nanoparticles, as the coordination numbers (Table in Figure 2 and Table S1) are significantly smaller than 12, which is typically expected for bulk fcc metals.

Furthermore, the refinements show that Pt and Ni are both surrounded by Ni and Pt, respectively. Moreover, a significant change in bond lengths due to the alloying is found: the Pt–Pt bond shrinks from 2.74 Å in Pt@HGS to 2.67 Å in PtNi@HGS whereas a Pt–Ni backscattering contribution is found at 2.60 Å. Interestingly, and in contrast from what is observed for the Pt L_3-edge, where the local environment consists only of Pt and Ni atoms, the EXAFS analysis of the Ni K-edge reveals a first coordination shell of carbon atoms at 1.95 ± 0.05 Å. Furthermore, the local order analysis shows a relatively higher disorder among the Ni–Ni and Ni–C bond lengths (Table S1). The Ni–C contribution may be attributed to the formation of a Ni-rich surface layer during synthesis that evolves into Ni carbide at the high annealing temperatures. We propose, based on the XRD, TEM, and EXFAS results, that after the alloying treatment the metallic nanoparticles have a Pt–Ni/Ni–C structure, with a disordered PtNi alloy as the core and a Ni–C skin as the outermost surface layer.

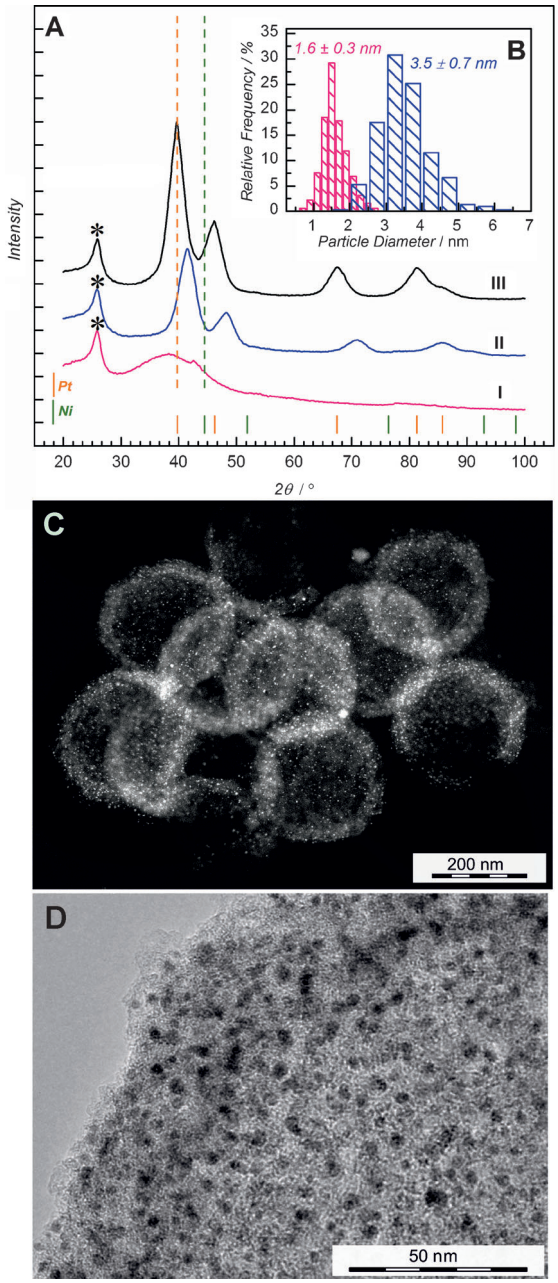

Figure 1. Catalyst characterization. A) XRD patterns of PtNi@HGS after the reduction (I) and after the annealing treatment (II). For comparison, the pattern of pure Pt@HGS is also shown (III). B) Particle size distribution histograms of the PtNi catalyst after reduction (violet) and after annealing (blue). C) STEM dark field overview and D) detailed TEM image of PtNi@HGS.

The electrochemical activity of the PtNi@HGS catalyst is summarized in Figure 3. Regular cyclic voltammograms with

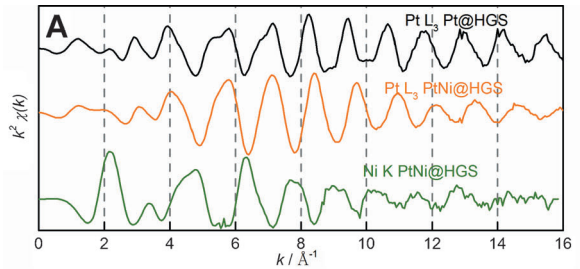

C

Sample	Edge	Shell	Atom	*N*	*r*(Å)
Pt-HGS		1st	Pt	9.3±0.7[f]	2.74[fʃ]
PtNi-HGS	Pt L_3	1st	Ni	4.8±0.8[f]	2.60[fʃ†]
		2nd	Pt	4.9±0.8[f]	2.67[fʃ]
	Ni K	1st	C	2.2±1.2[f]	1.95±0.05[f]
		2nd	Ni	3.0±2.4[f]	2.48[f ʃ]
		3rd	Pt	4.9±2.0[f]	2.60[f ʃ †]

ʃ= fitted uncertainity lower than 1%,f= fitted and s=fixed,
†=shared parameter during the fit. Structural parameters:
N=number of neighboring atoms, r= distance

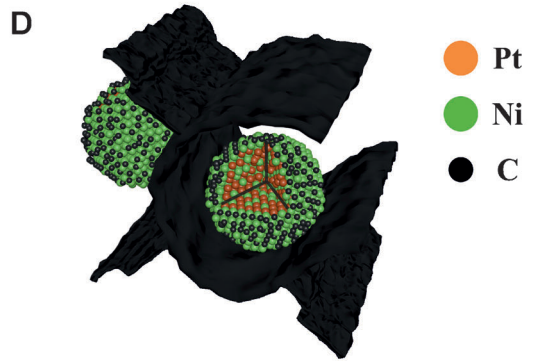

Figure 2. EXAFS model. A) k^2 weighted EXAFS spectra (Pt L_3-edge and Ni K-edge) for Pt@HGS and PtNi@HGS; B) corresponding k^2 weighted Fourier transforms. C) Table with essential parameters (N = coordination numbers, r = atomic distances) derived from EXAFS. ʃ = fitted uncertainty lower than 1%, f = fitted, s = fixed, † = shared parameter. D) 3D structural model of PtNi@HGS after annealing with the metal nanoparticles confined inside the carbon matrix.

clear Pt features can be obtained after an initial cleaning procedure in which the protective NiC is removed.[12] Although the nanoparticles are to a great extent inside the porous matrix of the support, they are still accessible for electrolyte and reactants, such as oxygen, and show a large ECSA of $108 \pm 10\ m^2 g_{Pt}^{-1}$. As expected from the effect of alloying, the specific activity of PtNi@HGS is about twofold higher than that of a standard Pt/Vulcan catalyst with a comparable particle size distribution. Moreover, owing to the exceptionally small particle size and thus high surface area for an alloy, the mass activity after the initial activation is enhanced by a factor of three ($1.0 \pm 0.04\ A\,mg_{Pt}^{-1}$), placing the PtNi@HGS among the most active Pt alloy catalysts available.[1a,3c] Note that although only fundamental RDE data is provided at this stage, the kinetic information obtained by this approach are typically well in line with single fuel-cell measurements, even on a quantitative level.[13] Moreover, the previously obtained results on Pt@HGS suggest that specific mass-transport resistances, which could be due to the confinement of the active particles in the support, do not occur even at high current densities.[10a] Therefore the PtNi@HGS can be also considered as an excellent candidate for real fuel cells after optimization of the electrode structure and membrane electrode assembly (MEA).

Since durability issues, particularly de-alloying, are a critical point for Pt alloy catalysts, the promising initial activity was additionally followed during an accelerated aging test within the operational window of an ORR catalyst. According to the CO-stripping and cyclic voltammograms recorded in argon, the initial surface area is quite low, which is mainly due to the presence of the residual Ni–C-rich layer covering the Pt surface after the synthesis. Remarkably, after activation and reaching the complete accessibility of the active platinum surface, further potential cycling in the potential range between 0.4 and 1.0 V_{RHE} at $1.0\ V\,s^{-1}$ does not significantly alter the cyclic voltammograms, so that the ECSA is constant over the remaining, extensive aging/degradation test (Figure 3B). After 10440 cycles the final ECSA value is 98% of the initial one, well within the uncertainty of the measurement, so that the catalyst can be considered as stable under these conditions. This is additionally supported by the completely retained specific activity for the ORR, measured before and after the series of 10000 cycles (Figure 3D). Thus it seems that not only the nanoparticles within the support structure do not coalesce nor detach, but also the overall nickel content remains high. To further confirm our initial findings, the evolution of the nickel content was also followed by monitoring the Ni leaching directly during the activation procedure utilizing online ICP-MS[14] (Figure 3E) and by post-use analysis of the RDE catalyst films (Figure 3B, inset).

As shown in Figure 3E, the alloying element is released to a minor extent upon initial contact with the electrolyte, most likely due to unalloyed Ni atoms or clusters, and more significantly during the activation cycles to positive potentials. However, once the activation is completed, further cycling between 0.05 and 1.0 V_{RHE} does not yield any detectable Ni leaching (Figure 3E), suggesting that the entire exposed nickel has been removed. Additionally, we quantitatively analyzed the RDE films after activation showing that the Ni content drops to $25 \pm 1\%$ (Figure 3B, Inset), which is consistent with other studies available in literature.[15] Most importantly, the Ni content appears to be rather stable even after the 10000 aging cycles, in line with the constant specific activity values previously shown. To directly observe the lack of degradation on the nanoscale, STEM and high-resolution EELS were performed on identical locations of the catalyst.[4] The HGS morphology as well as the PtNi particle size and size distribution indeed remain unaltered during 5000 potential cycles between 0.4 and 1.0 V_{RHE}. Moreover, qualitatively the Ni signal decreases only slightly after the aging procedure

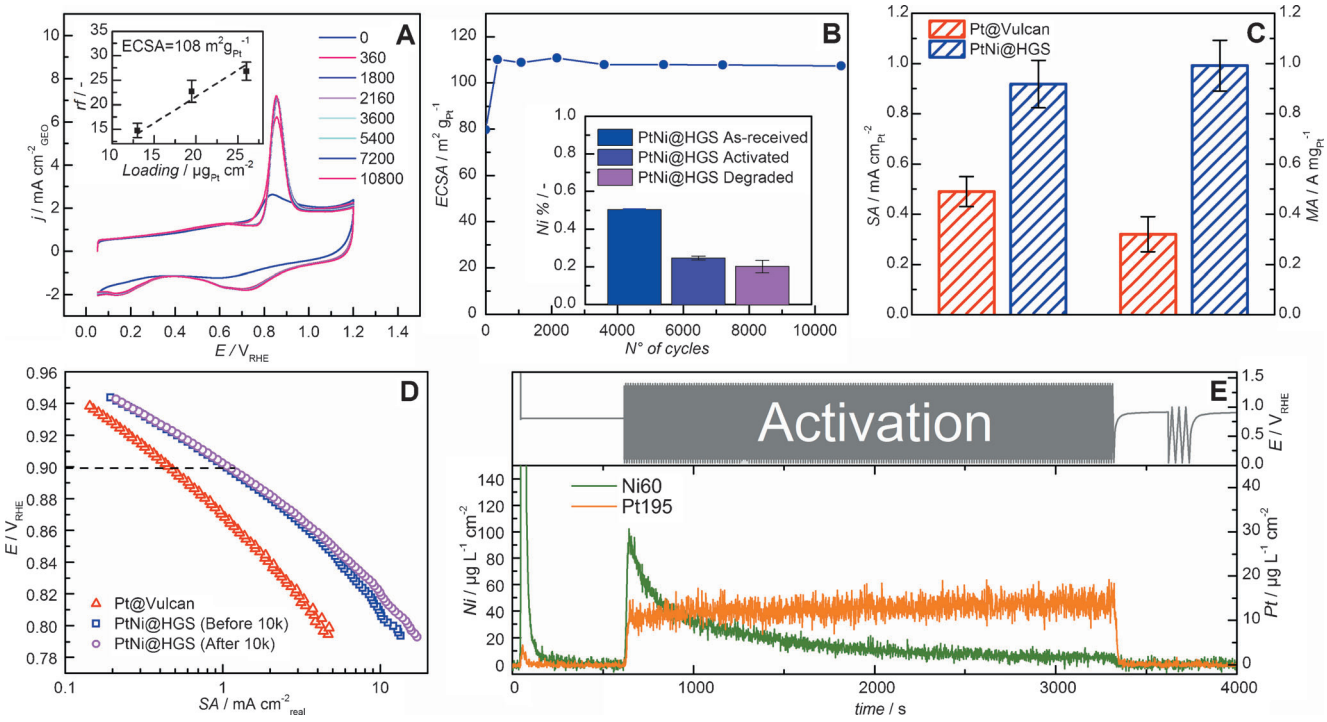

Figure 3. Assessment of the electrochemical activity and stability of PtNi@HGS. A) Evolution of the CO-stripping voltammograms throughout the aging step and ECSA determination from the slope of the roughness factor (rf) versus the catalyst loading (Inset); B) evolution of the ECSA over time and Ni ratio for the as-received, activated, and aged catalyst (Inset); C) specific activity (left axis) and mass activity (right axis) of PtNi@HGS and a standard Pt/Vulcan at 0.9 V_{RHE}; D) specific activity comparison by means of Tafel plots of the PtNi@HGS before and after the aging procedure to a standard Pt/Vulcan; E) online Ni and Pt leaching profile throughout the activation procedure, consisting of 200 cycles between 0.05 and 1.4 V_{RHE} with 0.2 Vs^{-1}, and 3 cycles between 0.05 and 1.0 V_{RHE} with 0.05 Vs^{-1}.

(Figure 4). These results complement the macroscopic electrochemical data and clearly confirm the stability of the catalyst within the applied potential window. Considering that the applied potentials are far above the equilibrium potential of Ni, both the results from ICP-MS and HR-EELS, can be explained by the presence of a Pt-rich outmost layer shielding the less-noble metal from dissolution in the core–shell structure formed upon initial de-alloying.

In conclusion, we have successfully synthesized a Pt alloy nanocatalyst of 3–4 nm in diameter with a narrow size distribution by space-confined alloying of Pt–Ni nanoparticles in the mesoporous structure of the support. The

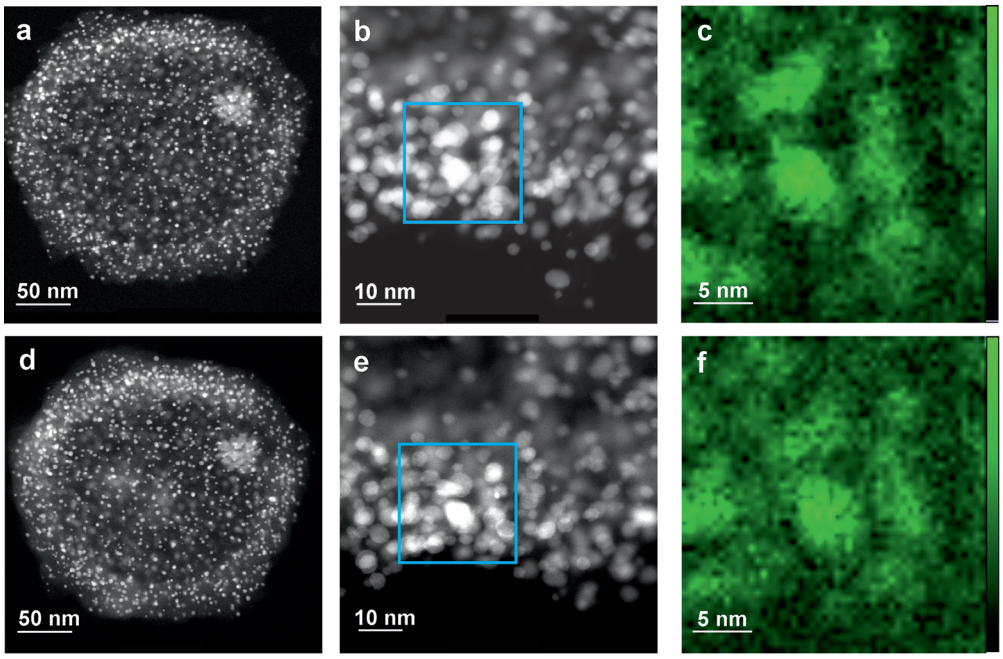

Figure 4. Following the effect of the aging on PtNi@HGS on the nanoscale. Images in the upper row show a representative scanning transmission electron microscopy (STEM) overview of a single hollow graphitic sphere (A), a section of the sphere shell (B), and an EELS map of the Ni signal (C) for the selected area (the blue square in (B)) before aging. Images in the bottom row (D–F) show the identical locations after 5000 potential cycles in 0.1 M $HClO_4$ between 0.4 and 1.0 V_{RHE} at room temperature.

PtNi@HGS yields a threefold increase in mass activity with respect to conventional catalysts, which would be equivalent to a threefold reduction of the required Pt mass and thus the cost for applications. Moreover, the Ni content of the activated catalyst remains nearly unaltered even after mild accelerated aging, and because of the pore confinement the particles neither detach nor coalesce. Thus, the enhanced activity is completely maintained after aging within the operation range of an ORR catalyst, which makes it a highly promising candidate for PEM fuel cells.

Experimental Section

The HGS were synthetized by a nanocasting route using core–shell mesoporous silica spheres as a hard template, divinylbenzene as the carbon precursor, and $Fe(NO_3)_3$ as a graphitization catalyst.[10a] All activities were extracted from CVs recorded in O_2-saturated electrolyte at 1600 rpm and at 0.9 V_{RHE}. The stability test included an activation step of 360 cycles between 0.4 and 1.4 V_{RHE} with 1 $V s^{-1}$. Further details on materials, methods and characterization are provided in the Supporting Information.

Received: July 2, 2014
Revised: August 18, 2014
Published online: October 29, 2014

Keywords: electrocatalysis · fuel cells · nanoparticles · stability

[1] a) M. K. Debe, *Nature* **2012**, *486*, 43 – 51; b) H. A. Gasteiger, N. M. Marković, *Science* **2009**, *324*, 48 – 49.
[2] M. Nesselberger, S. Ashton, J. C. Meier, I. Katsounaros, K. J. J. Mayrhofer, M. Arenz, *J. Am. Chem. Soc.* **2011**, *133*, 17428 – 17433.
[3] a) V. R. Stamenkovic, B. Fowler, B. S. Mun, G. Wang, P. N. Ross, C. A. Lucas, N. M. Marković, *Science* **2007**, *315*, 493 – 497; b) T. Toda, H. Igarashi, H. Uchida, M. Watanabe, *J. Electrochem. Soc.* **1999**, *146*, 3750 – 3756; c) A. Rabis, P. Rodriguez, T. J. Schmidt, *ACS Catal.* **2012**, *2*, 864 – 890; d) P. Strasser, S. Koh, T. Anniyev, J. Greeley, K. More, C. Yu, Z. Liu, S. Kaya, D. Nordlund, H. Ogasawara, M. F. Toney, A. Nilsson, *Nat. Chem.* **2010**, *2*, 454 – 460; e) L. Wei, R. Paramaconi, B. Lars, F. Annette, Y. Jipei, H. Anne-Kristin, G. Dorin, Z. Zhikun, K. Stefan, G. Nikolai, K. Rüdiger, J. S. Thomas, E. Alexander, *Angew. Chem. Int. Ed.* **2013**, *52*, 9849 – 9852; *Angew. Chem.* **2013**, *125*, 10033 – 10037.
[4] J. C. Meier, C. Galeano, I. Katsounaros, A. A. Topalov, A. Kostka, F. Schüth, K. J. J. Mayrhofer, *ACS Catal.* **2012**, *2*, 832 – 843.
[5] P. J. Ferreira, G. J. la O', Y. Shao-Horn, D. Morgan, R. Makharia, S. Kocha, H. A. Gasteiger, *J. Electrochem. Soc.* **2005**, *152*, A2256 – A2271.
[6] a) A. Bonakdarpour, K. Stevens, G. D. Vernstrom, R. Atanasoski, A. K. Schmoeckel, M. K. Debe, J. R. Dahn, *Electrochim. Acta* **2007**, *53*, 688 – 694; b) D. van der Vliet, C. Wang, M. Debe, R. Atanasoski, N. M. Markovic, V. R. Stamenkovic, *Electrochim. Acta* **2011**, *56*, 8695 – 8699.
[7] a) C. Cui, L. Gan, H.-H. Li, S.-H. Yu, M. Heggen, P. Strasser, *Nano Lett.* **2012**, *12*, 5885 – 5889; b) C. Wang, N. M. Markovic, V. R. Stamenkovic, *ACS Catal.* **2012**, *2*, 891 – 898.
[8] S. Shrestha, Y. Liu, W. E. Mustain, *Catal. Rev. Sci. Eng.* **2011**, *53*, 256 – 336.
[9] a) C. Wang, M. Chi, D. Li, D. Strmcnik, D. van der Vliet, G. Wang, V. Komanicky, K.-C. Chang, A. P. Paulikas, D. Tripkovic, J. Pearson, K. L. More, N. M. Markovic, V. R. Stamenkovic, *J. Am. Chem. Soc.* **2011**, *133*, 14396 – 14403; b) C. Wang, D. van der Vliet, K. L. More, N. J. Zaluzec, S. Peng, S. Sun, H. Daimon, G. Wang, J. Greeley, J. Pearson, A. P. Paulikas, G. Karapetrov, D. Strmcnik, N. M. Markovic, V. R. Stamenkovic, *Nano Lett.* **2011**, *11*, 919 – 926; c) K. Sasaki, H. Naohara, Y. Cai, Y. M. Choi, P. Liu, M. B. Vukmirovic, J. X. Wang, R. R. Adzic, *Angew. Chem. Int. Ed.* **2010**, *49*, 8602 – 8607; *Angew. Chem.* **2010**, *122*, 8784 – 8789; d) D. Wang, H. L. Xin, R. Hovden, H. Wang, Y. Yu, D. A. Muller, F. J. DiSalvo, H. D. Abruña, *Nat. Mater.* **2013**, *12*, 81 – 87; e) F. Hasché, M. Oezaslan, P. Strasser, *ChemCatChem* **2011**, *3*, 1805 – 1813; f) F. Hasché, M. Oezaslan, P. Strasser, *ECS Trans.* **2011**, *41*, 1079 – 1088; g) S. Guo, D. Li, H. Zhu, S. Zhang, N. M. Markovic, V. R. Stamenkovic, S. Sun, *Angew. Chem. Int. Ed.* **2013**, *52*, 3465 – 3468; *Angew. Chem.* **2013**, *125*, 3549 – 3552.
[10] a) C. Galeano, J. C. Meier, V. Peinecke, H. Bongard, I. Katsounaros, A. A. Topalov, A. Lu, K. J. J. Mayrhofer, F. Schüth, *J. Am. Chem. Soc.* **2012**, *134*, 20457 – 20465; b) WO2103117725, **2013**; c) WO2013117192, **2013**.
[11] a) A.-H. Lu, J.-J. Nitz, M. Comotti, C. Weidenthaler, K. Schlichte, C. W. Lehmann, O. Terasaki, F. Schuìth, *J. Am. Chem. Soc.* **2010**, *132*, 14152 – 14162; b) G. Prieto, J. Zečević, H. Friedrich, K. P. de Jong, P. E. de Jongh, *Nat. Mater.* **2013**, *12*, 34 – 39.
[12] K. J. J. Mayrhofer, D. Strmcnik, B. B. Blizanac, V. Stamenkovic, M. Arenz, N. M. Markovic, *Electrochim. Acta* **2008**, *53*, 3181 – 3188.
[13] H. A. Gasteiger, S. S. Kocha, B. Sompalli, F. T. Wagner, *Appl. Catal. B* **2005**, *56*, 9 – 35.
[14] M. J. Duarte, J. Klemm, S. O. Klemm, K. J. J. Mayrhofer, M. Stratmann, S. Borodin, A. H. Romero, M. Madinehei, D. Crespo, J. Serrano, S. S. A. Gerstl, P. P. Choi, D. Raabe, F. U. Renner, *Science* **2013**, *341*, 372 – 376.
[15] C. Wang, M. Chi, G. Wang, D. van der Vliet, D. Li, K. More, H.-H. Wang, J. A. Schlueter, N. M. Markovic, V. R. Stamenkovic, *Adv. Funct. Mater.* **2011**, *21*, 147 – 152.

